



HAL
open science

Crack models based on the extended finite element method

Nicolas Moës

► **To cite this version:**

Nicolas Moës. Crack models based on the extended finite element method. Numerical Modeling of Concrete Cracking, 532, Springer, pp.221-264, 2011, CISM International Centre for Mechanical Sciences, 10.1007/978-3-7091-0897-0_5. hal-04800217

HAL Id: hal-04800217

<https://hal.science/hal-04800217v1>

Submitted on 24 Nov 2024

HAL is a multi-disciplinary open access archive for the deposit and dissemination of scientific research documents, whether they are published or not. The documents may come from teaching and research institutions in France or abroad, or from public or private research centers.

L'archive ouverte pluridisciplinaire **HAL**, est destinée au dépôt et à la diffusion de documents scientifiques de niveau recherche, publiés ou non, émanant des établissements d'enseignement et de recherche français ou étrangers, des laboratoires publics ou privés.



Distributed under a Creative Commons Attribution - NonCommercial 4.0 International License

Crack models based on the extended finite element method

Nicolas Moës

GeM Institute, UMR CNRS 6183, Ecole Centrale de Nantes, France

1 Introduction

In spite of its decades of existence, the finite element method coupled with meshing tools does not yet manage to simulate efficiently the propagation of 3D cracks for geometries relevant to engineers in industry. Indeed, initial creation of the mesh and modification of this mesh during the propagation of a crack, remain extremely heavy and lack robustness. This fact was the motivation behind the design of the eXtended Finite Element Method (X-FEM).

Even if this operation were straightforward, the question of the projection of fields from one mesh to the next one would still be raised for history dependent problems (plasticity, dynamics, ...). The possibility offered to preserve the mesh through the simulation is undoubtedly appealing.

The basic idea is to introduce inside the elements the proper discontinuities so as to relax the need for the mesh to conform to them. This introduction is done via the technique of the partition of unity (Melenk and Babuška, 1996; Babuška and Melenk, 1997). It should be noted that X-FEM is not the only method based on the partition of the unity (as in painting several schools exist). The GFEM approach (generalized finite element method) and PUFEM (partition of unity finite element method) are also based on the partition of unity.

The constant ambition which distinguishes the X-FEM approach since its beginnings is to use the partition of unity to release the mesh from constraints to conform to surfaces of discontinuity, while keeping the same performance as traditional finite element (optimality of convergence). Quickly also the X-FEM was coupled to the level set method to locate and evolve the position of surfaces of discontinuities.



Figure 1. Reference problem.

2 Background on discretization methods

2.1 Problem description and notations

The solid studied is depicted in Figure 1. It occupies a domain Ω whose boundary is denoted by S . This boundary is composed of the crack faces S_{c-} and S_{c+} assumed traction free, as well as a part S_u on which displacement \mathbf{u}^* are imposed and, finally, a part S_t on which tractions \mathbf{t}^* are imposed.

Stresses, strains and displacements are denoted by $\boldsymbol{\sigma}$, $\boldsymbol{\varepsilon}$ and \mathbf{u} , respectively. Small strains and displacements are assumed throughout the chapter. In the absence of volume forces, equilibrium equations read

$$\nabla \cdot \boldsymbol{\sigma} = 0 \quad \text{on } \Omega \quad (1)$$

$$\boldsymbol{\sigma} \cdot \mathbf{n} = \mathbf{t}^* \quad \text{on } S_t \quad (2)$$

$$\boldsymbol{\sigma} \cdot \mathbf{n} = 0 \quad \text{on } S_{c+}, \quad \boldsymbol{\sigma} \cdot \mathbf{n} = 0 \quad \text{on } S_{c-} \quad (3)$$

where \mathbf{n} is the outward normal. Kinematics equations read

$$\boldsymbol{\varepsilon} = \boldsymbol{\varepsilon}(\mathbf{u}) = \nabla_s \mathbf{u} \quad \text{on } \Omega \quad (4)$$

$$\mathbf{u} = \mathbf{u}^* \quad \text{on } S_u \quad (5)$$

where ∇_s is the symmetrical part of the gradient operator. Finally, the constitutive law is assumed elastic: $\boldsymbol{\sigma} = \mathbf{E} : \boldsymbol{\varepsilon}$ where \mathbf{E} is Hooke's tensor. The space of admissible displacement field is denoted U . whereas the space of admissible virtual displacements is denoted U_0 :

$$U = \{ \mathbf{v} \text{ regular} : \mathbf{v} = \mathbf{u}^* \text{ on } S_u \} \quad (6)$$

$$U_0 = \{ \delta \mathbf{v} \text{ regular} : \delta \mathbf{v} = 0 \text{ on } S_u \} \quad (7)$$

The regularity space to which the solution belongs is detailed in (Babuška and Rosenzweig, 1972) and (Grisvard, 1985). This space contains discontinuous fields of displacement across the crack faces S_c . The weak form of the equilibrium equations is written

$$\int_{\Omega} \boldsymbol{\sigma} : \boldsymbol{\varepsilon}(\delta \mathbf{u}) \, d\Omega = \int_{S_t} \mathbf{t}^* \cdot \delta \mathbf{u} \, dS \quad \forall \delta \mathbf{u} \in U_0 \quad (8)$$

Let us note that the border S_c does not contribute to the weak form because it is traction free (this assumption will be released later). Combining (8) with the constitutive law and the kinematics equations, the displacement variational principle is obtained. Find $\mathbf{u} \in U$ such that

$$\int_{\Omega} \boldsymbol{\varepsilon}(\mathbf{u}) : \mathbf{E} : \boldsymbol{\varepsilon}(\delta \mathbf{u}) \, d\Omega = \int_{S_t} \mathbf{t}^* \cdot \delta \mathbf{u} \, dS \quad \forall \delta \mathbf{u} \in U_0 \quad (9)$$

2.2 Rayleigh-Ritz approximation

Within the Rayleigh-Ritz method, the approximation is written as a linear combination of displacement modes $\boldsymbol{\phi}_i(\mathbf{x})$, $i = 1, \dots, N$ defined on the domain of interest:

$$\mathbf{u}(\mathbf{x}) = \sum_i^N a_i \boldsymbol{\phi}_i(\mathbf{x}) \quad (10)$$

These modes must satisfy *a priori* the essential boundary conditions (imposed displacements are considered null to simplify the presentation). The introduction of this approximation into the variational principle (9) leads to the following system of equations

$$K_{ij} a_j = f_i, \quad j = 1, \dots, N \quad (11)$$

The summation rule over repeated indices is assumed.

$$K_{ij} = \int_{\Omega} \boldsymbol{\varepsilon}(\boldsymbol{\phi}_i) : \mathbf{E} : \boldsymbol{\varepsilon}(\boldsymbol{\phi}_j) \, d\Omega \quad (12)$$

$$f_i = \int_{S_t} \mathbf{t}^* \cdot \boldsymbol{\phi}_i \, dS \quad (13)$$

The method of Rayleigh-Ritz offers a great freedom in the choice of the modes. These modes can for example be selected so as to satisfy the interior equations. However, this method has the disadvantage of leading to a linear system with dense matrix, on contrary to the finite element method which leads to a sparse system.

2.3 The finite element method

In the finite element method, the domain of interest, Ω , is broken up into geometrical subdomains of simple shape Ω_e , $e = 1, \dots, N_e$ called elements:

$$\Omega = \cup_{e=1}^{N_e} \Omega_e \quad (14)$$

The set of elements constitutes the mesh. On each element, the unknown field is approximated using simple approximation functions, of polynomial type, as well as unknown coefficients called degrees of freedom. Degrees of freedom have a simple mechanical significance in general. For linear elements, the degrees of freedom are simply the displacement of the nodes along x and y directions. Let us indicate by u_i^α the displacement of node i in direction α ($\alpha = x$ or y) and by ϕ_i^α the corresponding approximation function. The finite element approximation on element Ω_e is written

$$\mathbf{u}(\mathbf{x})|_{\Omega_e} = \sum_{i \in N_n} \sum_{\alpha} a_i^\alpha \phi_i^\alpha(\mathbf{x}) \quad (15)$$

where N_n denotes the set of nodes of element Ω_e . For instance, for a triangle, they are six approximation functions

$$\{\phi_i^\alpha\} = \{\phi_1 \mathbf{e}_x, \phi_2 \mathbf{e}_x, \phi_3 \mathbf{e}_x, \phi_1 \mathbf{e}_y, \phi_2 \mathbf{e}_y, \phi_3 \mathbf{e}_y\} \quad (16)$$

where ϕ_1 , ϕ_2 and ϕ_3 are scalar linear functions over the element with value of 0 or 1 at the nodes. Approximation (15) allows one to model any rigid mode or constant strain over the element. This condition must be fulfilled by the approximation for any type of elements. Continuity of the approximation over the domain is obtained by the use of nodal degrees of freedom shared by all elements connected to the node. The stiffness matrix, K_{ij}^e , and load vector, f_i^e , are given for a finite element by

$$K_{i\alpha, j\beta}^e = \int_{\Omega^e} \boldsymbol{\varepsilon}(\phi_i^\alpha) : \mathbf{E} : \boldsymbol{\varepsilon}(\phi_j^\beta) \, d\Omega \quad (17)$$

$$f_{i\alpha}^e = \int_{S_t \cap \partial\Omega^e} \mathbf{t}^* \cdot \phi_i^\alpha \, dS \quad (18)$$

The global system of equations is obtained by assembling the elementary matrices and forces in a global stiffness and force vector. In the assembly process, the equations related to degrees of freedom involved in Dirichlet boundary conditions are not built.

On the contrary to the Rayleigh-Ritz approximation, the local character of the finite element approximation leads to sparse matrices. Moreover, the finite element has a strong mechanical interpretation: kinematics is described by nodal displacements which are associated by duality to nodal forces. The behavior of the element is characterized by the elementary stiffness matrix which connects the nodal forces and displacements. The global system to solve enforces the equilibrium of the structure: the sum of the nodal forces at each node must be zero. Lastly, the finite element

method did demonstrate a high level of robustness in industry which makes it a very appropriate approach for most applications.

However, the use of the finite element method for problems with complex geometry or evolution of internal surfaces is currently obstructed by meshing issues. This did yield a motivation to design the so called meshless methods.

2.4 Meshless methods

We give some insights on meshless methods because they are important to understand the history of the concept of enrichment. Within the framework of meshless methods, the support of the approximation function is more important than the elements (which actually do not exist any more). On these supports, enrichment functions may be introduced for example to model a crack tip (as in (Fleming et al., 1997)).

Years of active research on meshless methods did show the importance of the support. Many researches were undertaken in the nineties to develop methods in which the approximation does not rest on a mesh but rather on a set of points. Various methods exist to date: diffuse elements (Nayroles et al., 1992), Element Free Galerkin method (EFG) (Belytschko et al., 1994), Reproducing Kernel Particle Method (RKPM) (Liu et al., 1993), $h-p$ cloud method (Duarte and Oden, 1996).

Each point has a domain of influence (support) with a simple shape (circle or rectangle for example in 2D) on which approximations are built. These functions are zero on the boundary and outside the domain of influence. Abusively, we will speak about the support i for the support associated with node i . The approximation functions defined on the support i are denoted ϕ_i^α , $\alpha = 1, \dots, N_f(i)$ where $N_f(i)$ is the number of functions defined over support i . The corresponding degrees of freedom are denoted a_i^α . The approximation at a given point \mathbf{x} is written

$$\mathbf{u}(\mathbf{x}) = \sum_{i \in N_s(\mathbf{x})} \sum_{\alpha=1}^{N_f(i)} a_i^\alpha \phi_i^\alpha(\mathbf{x}) \quad (19)$$

where $N_s(\mathbf{x})$ is the set of points whose support contains point \mathbf{x} . Figure 2 shows for example a point \mathbf{x} covered by three supports. The approximation functions are built so that the approximation (19) can represent all rigid modes and constant strain modes on the domain. These conditions are necessary to prove the convergence of the method. Various approaches (diffuse element, EFG, RKPM, ...) are distinguished, among other things, by the techniques used for the construction of these approximation functions.

Once a set of approximation functions has been built, it is possible to add some by enrichment. Various manners of enriching exist and we will describe

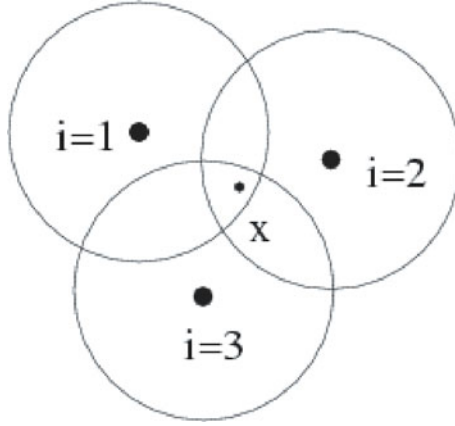


Figure 2. Three supports covering node \mathbf{x} .

an enrichment type described as external by Belytschko and Fleming (1999). The enrichment of the approximation makes it possible to represent a given displacement mode, for example $F(\mathbf{x})\mathbf{e}_x$ on a subdomain denoted by $\Omega_F \subset \Omega$. Let us note N_F the set of supports which have a non empty intersection with Ω_f . The enriched approximation is written

$$\mathbf{u}(\mathbf{x}) = \sum_{i \in N_s(\mathbf{x})} \sum_{\alpha=1}^{N_f(i)} a_i^\alpha \phi_i^\alpha(\mathbf{x}) + \sum_{i \in N_s(\mathbf{x}) \cap N_F} \sum_{\alpha=1}^{N_f(i)} b_i^\alpha \phi_i^\alpha(\mathbf{x}) F(\mathbf{x}) \quad (20)$$

where the new degrees of freedom, b_i^α , multiply the enriched approximation functions $\phi_i^\alpha(\mathbf{x})F(\mathbf{x})$. Let us show that the function $F(\mathbf{x})\mathbf{e}_x$ may be represented on Ω_f . By setting to zero all degrees of freedom a_i^α and taking the function $F(\mathbf{x})$ out of the sum, the approximation at point $\mathbf{x} \in \Omega_F$ reads

$$\mathbf{u}(\mathbf{x}) = \left(\sum_{i \in N_s(\mathbf{x}) \cap N_F} \sum_{\alpha=1}^{N_f(i)} b_i^\alpha \phi_i^\alpha(\mathbf{x}) \right) F(\mathbf{x}) \quad (21)$$

The degrees of freedom b_i^α can be selected so that the factor in front of $F(\mathbf{x})$ is the rigid mode \mathbf{e}_x . That is possible since functions ϕ_i^α are able to represent any rigid mode. In conclusion, approximation (20) can represent $F(\mathbf{x})\mathbf{e}_x$ on Ω_F . Enrichment made it possible within the framework of the Element Free Galerkin Method to solve problems of propagation of cracks in

two and three dimensions without remeshing (Krysl and Belytschko, 1999): the crack is propagated through a set of points and is modeled by enrichment of the approximation with discontinuous functions $F(\mathbf{x})$ on the crack or representing the singularity on the crack front. Great flexibility in the writing of the approximation and its enrichment as well as the possibility of creating very regular fields of approximation are two important assets of meshless methods and the EFG approach in particular. The use of meshless methods however presents a certain number of difficulties compared to the finite element method:

- Within the finite element method the assembly of the stiffness matrix can be done by assembling the contributions of each element. In meshless methods, the assembly is done rather by covering the domain by points of integration and by adding the contribution of each one of them. The choice of the position and the number of integration points is tedious for an arbitrary set of approximation points;
 - the approximation functions are to be built and are not explicit;
 - the support size is a parameter in the method which the user must choose carefully;
 - the boundary conditions of the Dirichlet type are delicate to impose.
- Finally, it must be pointed out that due to the lack of the element concept, meshless methods are not at all trivial to implement in legacy finite element codes.

2.5 The partition of unity

Melenk et Babuška (1996) did show that the traditional finite element approximation could be enriched so as to represent a specified function on a given domain. Their point of view can be summarized as follows. Let us first us recall that the finite element approximation is written on an element as

$$\mathbf{u}(\mathbf{x}) |_{\Omega_e} = \sum_{i \in N_n} \sum_{\alpha} a_i^{\alpha} \phi_i^{\alpha}(\mathbf{x}) \quad (22)$$

Since the degrees of freedom defined at a node have the same value for all the elements connected to it. The approximations on each element can be “assembled” to give a valid approximation in any point \mathbf{x} of the domain:

$$\mathbf{u}(\mathbf{x}) = \sum_{i \in N_n(\mathbf{x})} \sum_{\alpha} a_i^{\alpha} \phi_i^{\alpha}(\mathbf{x}) \quad (23)$$

where $N_n(\mathbf{x})$ is the set of nodes belonging to the elements containing point \mathbf{x} . The domain of influence (support) of the approximation function ϕ_i^{α} is the set of elements connected to node i . The set $N_n(\mathbf{x})$ is thus also the set of

nodes whose support covers point \mathbf{x} . The finite element approximation (23) can thus be interpreted as a particularization of the approximation (19) used in meshless methods:

- The set of points is the set of nodes in the mesh;
- The domain of influence of each node is the set of elements connected to it.

It is thus possible to enrich the finite element approximation by the same techniques as those used in meshless methods. Here is the enriched approximation which makes it possible to represent function $F(\mathbf{x})\mathbf{e}_x$ on domain Ω_F :

$$\mathbf{u}(\mathbf{x}) = \sum_{i \in N_n(\mathbf{x})} \sum_{\alpha} \phi_i^{\alpha} a_i^{\alpha} + \sum_{i \in N_n(\mathbf{x}) \cap N_F} \sum_{\alpha} b_i^{\alpha} \phi_i^{\alpha}(\mathbf{x}) F(\mathbf{x}) \quad (24)$$

where N_F is the set of nodes whose support has an intersection with domain Ω_F . The proof is obtained by setting to zero coefficients a_i^{α} and by taking into account the fact that the finite element shape functions are able to represent all rigid modes and thus the \mathbf{e}_x mode. We move now to the concrete use of the partition of unity for modeling discontinuities.

3 Discontinuity modeling with the X-FEM and level sets

The X-FEM introduces discontinuity inside elements using an enrichment based on the partition of unity technique. Proper enrichments for displacement discontinuities due to cracks will be discussed in this section. Proper enrichment for strain discontinuity may also be found in the literature as in (Moës et al., 2003).

3.1 A simple 1D problem

We consider a bar shown in Figure 3. Two cases are considered : a crack is located at a node or between two nodes.

Case a : crack located at a node Using classical finite elements, this case is treated using double nodes. Node 2 is replaced by nodes 2^- and 2^+ sharing the same location but bearing different unknowns as shown in Figure 4. The approximation reads

$$u = u_1 N_1 + u_2^- N_2^- + u_2^+ N_2^+ + u_3 N_3 + u_4 N_4 \quad (25)$$

where N_i indicates the approximation functions and u_i the corresponding degrees of freedom. Defining the displacement average, $\langle u \rangle$, and (half)

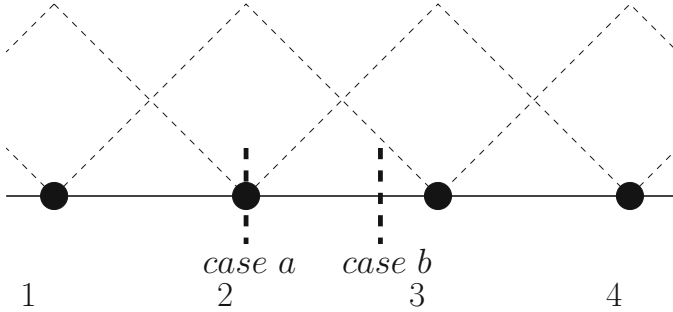


Figure 3. A bar with a crack located at a node (case a) or between two nodes (case b).

jump, $[u]$, at node 2

$$\langle u \rangle = \frac{u_2^- + u_2^+}{2} \quad [u] = \frac{u_2^- - u_2^+}{2} \quad (26)$$

the approximation may be rewritten as

$$u = u_1 N_1 + \langle u \rangle N_2 + [u] N_2 H(x) + u_3 N_3 \quad (27)$$

where

$$N_2 = N_2^- + N_2^+ \quad (28)$$

The generalized Heaviside function H (generalized because the original Heaviside function goes from 0 to 1) is represented in Figure 5. Abusively, we shall however call it Heaviside function. In the approximation (27), one distinguishes the continuous part modeled by functions N_1 , N_2 and N_3 to which is added a discontinuous part given by the product of N_2 by the Heaviside function. Node 2 is called an enriched node because an additional degree of freedom is given to it.

Case b: crack located in between two nodes Let us study now case b, Figure 3, in which the crack is located between two nodes. As in case a, we wish to write the approximation as the sum of a continuous and a discontinuous part. Evolving on case a, we propose

$$u = u_1 N_1 + u_2 N_2 + u_3 N_3 + u_4 N_4 + a_2 N_2 H + a_3 N_3 H \quad (29)$$

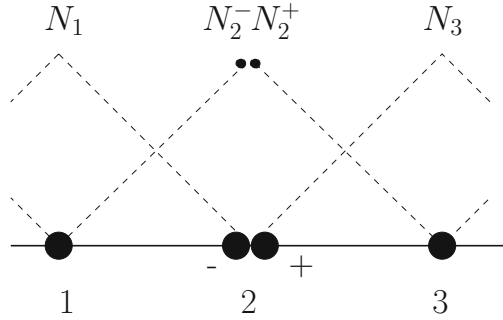


Figure 4. Double node to model a discontinuity located at a node.

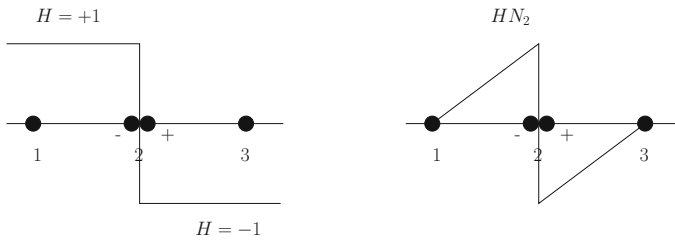


Figure 5. The generalized Heaviside function (left) as well as its product with function N_2 (right).

Nodes 2 and 3 are enriched by the Heaviside function. This enrichment was presented first (in 2D) by Moës et al. (1999). If the crack is located at a node, there is only one enriched node. In case b, two nodes are enriched because the support of nodes 2 and 3 are cut by the crack. A node is enriched by the Heaviside function if its support is cut into two by the crack. One can show that the approximation (29) makes it possible to represent two rigid modes (to the left of the crack and the other to the right). The fact that two (and not one) additional degrees of freedom are necessary may be surprising. Indeed, a crack implies a jump in displacement but can also imply a jump in strain. By linear combination of the various functions implied in (29), one notices that enrichment brings two functions on the element joining nodes 2 and 3. These two functions are shown in Figure 7. Note that for case a, only one additional degree of freedom is needed because finite element

already exhibits strain jumps across element boundaries.

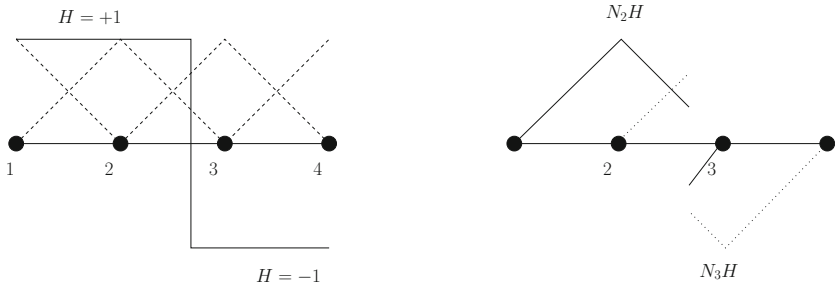


Figure 6. A crack located between two nodes. The Heaviside function (left) and enrichment functions (right).

Finally, it should be noted that proposed enrichment yields the same approximation space as if the cracked element is replaced by two elements and a double node. This observation is limited to 1D and will not carry over to 2D and 3D.

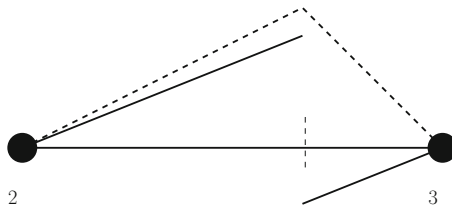


Figure 7. Two functions modeled by the X-FEM enrichment. We observe a continuous function with discontinuous slope (dashed line) and a discontinuous function with continuous slope (solid line).

Note that a set of variants to the Heaviside enrichment has been proposed in the literature: the “Hansbo” alternative (Hansbo and Hansbo, 2002), the use of virtual or phantom nodes (Molino et al., 2004), (Song et al., 2006) and, finally, the shifted basis from Zi and Belytschko (2003). All the variants listed above will lead to the same numerical solutions as the Heaviside enrichment described earlier. The choice is guided in general by the simplicity of implementation according to the target code. Also note

that even if these various bases will lead to the same solution, the generated matrices will not be identical (and will not have the same condition number).

3.2 Extension to 2D and 3D

We consider now 2D and 3D meshes cut by a crack. Just like in the 1D case, we begin with the case of a crack inserted with double nodes.

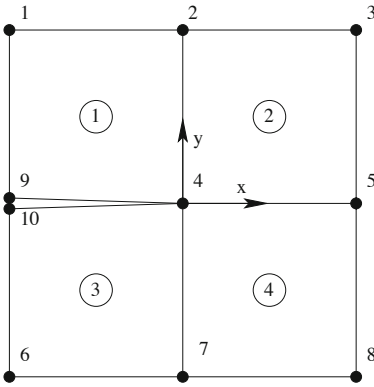


Figure 8. Finite element mesh near a crack tip, the circled numbers are element numbers

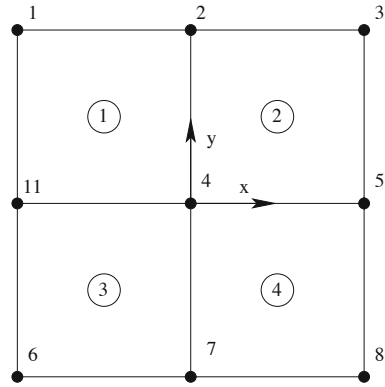


Figure 9. Regular mesh without a crack.

Figure 8 is taken from (Moës et al., 1999) and shows a four element mesh in which a crack has been introduced through double nodes (nodes 9 and 10). The finite element approximation associated with the mesh in Figure 8 is

$$\mathbf{u} = \sum_{i=1}^{10} \mathbf{u}_i N_i \quad (30)$$

where \mathbf{u}_i is the (vectorial) displacement at node i and ϕ_i is the bilinear shape function associated with node i . Each shape function ϕ_i has a compact support ω_i given by the union of the elements connected to node i .

Let us rewrite (30) in such a way that we recover an approximation without crack corresponding to Figure 9 and a discontinuous additional displacement. Defining the average displacement \mathbf{a} and the displacement jump \mathbf{b} on the crack faces as

$$\mathbf{a} = \frac{\mathbf{u}_9 + \mathbf{u}_{10}}{2} \quad \mathbf{b} = \frac{\mathbf{u}_9 - \mathbf{u}_{10}}{2} \quad (31)$$

we can express \mathbf{u}_9 and \mathbf{u}_{10} in terms of \mathbf{a} and \mathbf{b}

$$\mathbf{u}_9 = \mathbf{a} + \mathbf{b} \quad \mathbf{u}_{10} = \mathbf{a} - \mathbf{b} \quad (32)$$

Then replacing \mathbf{u}_9 and \mathbf{u}_{10} in terms of \mathbf{a} and \mathbf{b} in (30) yields

$$\mathbf{u} = \sum_{i=1}^8 \mathbf{u}_i N_i + \mathbf{a}(N_9 + N_{10}) + \mathbf{b}(N_9 + N_{10})H(\mathbf{x}) \quad (33)$$

where $H(\mathbf{x})$ is referred to here as a discontinuous, or ‘jump’ function. This is defined in the local crack coordinate system as

$$H(x, y) = \begin{cases} +1 & \text{for } y > 0 \\ -1 & \text{for } y < 0 \end{cases} \quad (34)$$

If we now consider the mesh in Figure 9, $N_9 + N_{10}$ can be replaced by N_{11} , and \mathbf{a} by \mathbf{u}_{11} . The finite element approximation now reads

$$\mathbf{u} = \sum_{i=0}^8 \mathbf{u}_i N_i + \mathbf{u}_{11} N_{11} + \mathbf{b} N_{11} H(\mathbf{x}) \quad (35)$$

First two terms on the right hand side represent the classical finite element approximation, whereas the last one represents the addition of a discontinuous enrichment. In other words, when a crack is modeled by a mesh as in Figure 8, we may interpret the finite element space as the sum of one which does not model the crack (such as Figure 9) and a discontinuous enrichment. The third term may be interpreted as an enrichment of the finite element function by a partition of unity technique.

Derivation that we have just carried out on a small grid of four elements may be reiterated on any 1D, 2D or 3D grid containing a discontinuity modeled by double nodes. This derivation will yield to the same conclusion: the modeling of a discontinuity by double nodes is equivalent to a traditional finite element modeling to which an enrichment by the partition of unity of the nodes located on the path of discontinuity is added. Let us note that the nodes which are enriched are characterized by the fact that their support is cut into two by the discontinuity.

Let us suppose now that one wishes to model a discontinuity which does not follow the edge of the elements. We propose to enrich all the nodes whose support is (completely) cut into two by the discontinuity (Moës et al., 1999). At these nodes, we add a degree of freedom (vectorial if the field is vectorial) acting on the traditional shape function at the node multiplied by a discontinuous function $H(\mathbf{x})$ being 1 on a side of the crack and -1 on

the other. For example, in Figures 10 and 11, circled nodes are enriched. A node whose support is not completely cut by discontinuity must not be enriched by function H because that would result in enlarging the crack artificially. For example, for the mesh shown in Figure 11, if nodes C and D are enriched, the crack will be active up to the point R (since the displacement field will be discontinuous up to point R). However, if only nodes A and B are enriched by the discontinuity, the displacement field is discontinuous only up to point Q and the crack appears unfortunately shorter.

In order to represent the crack on its proper length, nodes whose support contains the crack tip (squared nodes shown in Figure 11) are enriched with discontinuous functions up to the crack tip but not beyond. Such functions are provided by the asymptotic modes of displacement (elastic if calculation is elastic) at the crack tip. This enrichment, already used by Belytschko and Black (1999) and Strouboulis et al. (2000) allows moreover precise calculations since the asymptotic characteristics of the displacement field are built-in. Let us note that if the solution is not singular at the crack tip (for example by the presence of a cohesive zone), other functions of enrichment can be selected (Moës and Belytschko, 2002; Zi and Belytschko, 2003).

We are now able to detail the complete modeling of a crack with X-FEM located arbitrarily on a mesh, Figure 12. The enriched finite element approximation is written:

$$\begin{aligned} \mathbf{u}^h(\mathbf{x}) &= \sum_{i \in I} \mathbf{u}_i N_i(\mathbf{x}) + \sum_{i \in L} \mathbf{a}_i N_i(\mathbf{x}) H(\mathbf{x}) \\ &+ \sum_{i \in K_1} N_i(\mathbf{x}) \left(\sum_{l=1}^4 \mathbf{b}_{i,1}^l F_1^l(\mathbf{x}) \right) + \sum_{i \in K_2} N_i(\mathbf{x}) \left(\sum_{l=1}^4 \mathbf{b}_{i,2}^l F_2^l(\mathbf{x}) \right) \end{aligned} \quad (36)$$

where:

- I is the set of nodes in the mesh;
- \mathbf{u}_i is the classical (vectorial) degree of freedom at node i ;
- N_i is the scalar shape function associated to node i ;
- $L \subset I$ is the subset of nodes enriched by the Heaviside function. The corresponding (vectorial) degrees of freedom are denoted \mathbf{a}_i . A node belongs to L if its support is cut in two by the crack and does not contain the crack tip. Those nodes are circled on Figure 12;
- $K_1 \subset I$ et $K_2 \subset I$ are the set of nodes to enrich to model crack tips numbered 1 and 2, respectively. The corresponding degrees of freedom are $\mathbf{b}_{i,1}^l$ and $\mathbf{b}_{i,2}^l$, $l = 1, \dots, 4$. A node belongs to K_1 (resp. K_2) if its

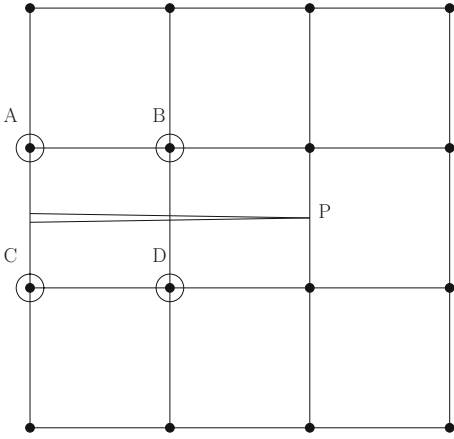


Figure 10. Crack not aligned with a mesh, the circled nodes are enriched with the discontinuous function $H(\mathbf{x})$.

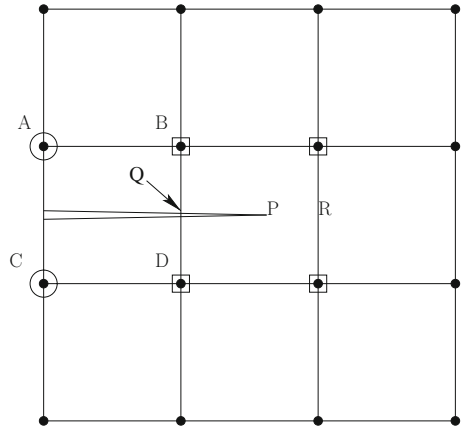


Figure 11. Crack not aligned with a mesh, the circled nodes are enriched with the discontinuous $H(\mathbf{x})$ function and the squared nodes with the tip enrichment functions.

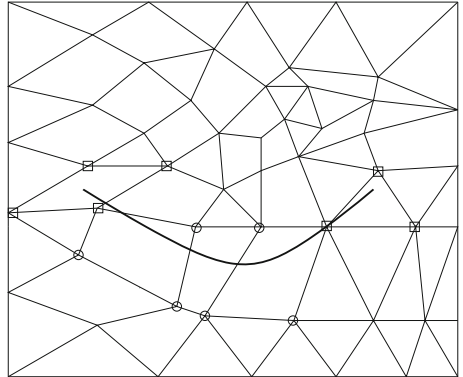
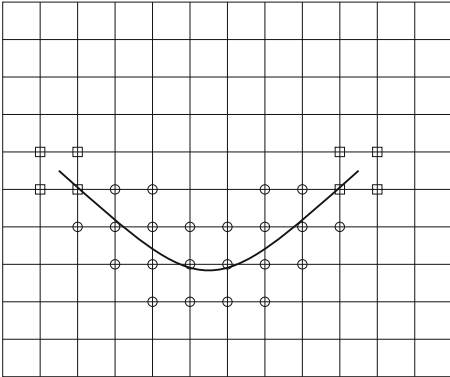


Figure 12. Crack located on a structured (left) and unstructured mesh (right). Circled nodes are enriched with the Heaviside function while squared nodes are enriched by tip functions.

support contains the first (resp. second) crack tip. Those nodes are squared in Figure 12.

Functions $F_1^l(\mathbf{x})$, $l = 1, \dots, 4$ modeling the crack tip are given in elasticity by:

$$\{F_1^l(\mathbf{x})\} \equiv \{\sqrt{r}\sin(\frac{\theta}{2}), \sqrt{r}\cos(\frac{\theta}{2}), \sqrt{r}\sin(\frac{\theta}{2})\sin(\theta), \sqrt{r}\cos(\frac{\theta}{2})\sin(\theta)\} \quad (37)$$

where (r, θ) are the polar coordinates in local axis at the crack tip. It must be noted that the first function is discontinuous across the crack. The three others are able to model strain discontinuity across the crack fraces. Similarly, functions $F_2^l(\mathbf{x})$ are also given by (37); the local system of coordinates being now locate around the second crack tip.

The extension to the three-dimensional case of the modeling of cracks by X-FEM was carried out in (Sukumar et al., 2000). Just like in the two-dimensional case, the fact that a node is enriched or not and the type of enrichment depend on the relative position of the support associated with the node compared to the crack location. The support of a node is a volume, the crack front is a curve (or several disjoint curves) and the crack itself is a surface. Enrichment functions for the crack front remain given by (37). A node is enriched if its support is touched by the crack front. The evaluation of r and θ can be done by finding the nearest point on the crack front, then by establishing a local base there. The use of level sets dealt with in the following section makes it possible to avoid this operation.

3.3 Cracks located by level sets

To locate a curve in 2D, one can indicate all points located on this curve for example using a parametric equation. One can qualify this representation as explicit. Another manner, implicit, to represent the curve is to consider it as the iso-zero level of a signed distance function. The distance is counted positively if one is inside the curve and negatively in the contrary case (the curve is supposed to separate the space in two zones). On a finite element mesh the level set is interpolated between the nodes by traditional finite element shape functions. In short, the location of a surface in 3D (curve in 2D) is given by a finite element field defined near the surface (curve). The knowledge of the signed distance is indeed needed in a narrow band around the surface.

For instance, in the Figure 13 one can see the value of a level set locating a circle on a grid (negative inside the circle and positive outside). The iso-zero contour of the level set function indicates the position of the circle. The level set is defined likewise in 3D. Figure 14 gives for example the iso-zero for a level set defined on a fine grid. The level set locates the material interface between strands and matrix in a so-called 4D composite.

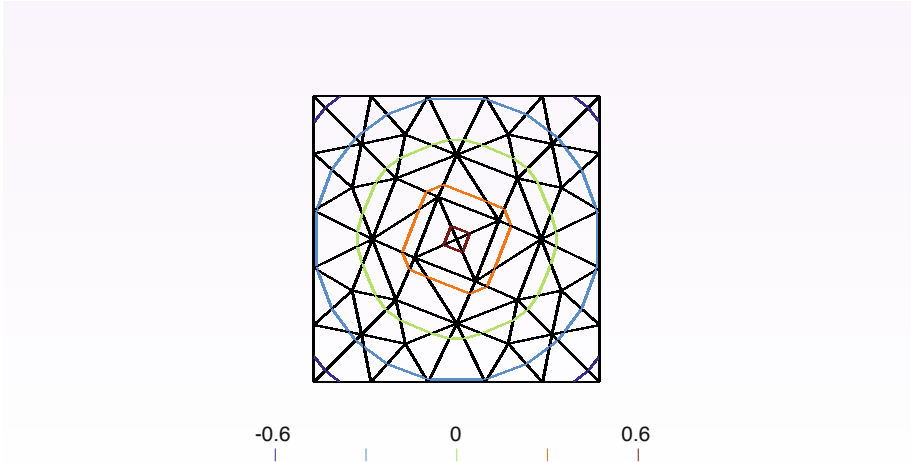


Figure 13. A level set locating a circle of radius 0.7 in a 2 by 2 plate. Five contours are plotted with level set values of -0.6, -0.3, 0.0, 0.3 and 0.6

As we indicated above, a level set separates space in two zones, a positive zone and a negative zone. A crack does not separate a domain into two (unless it is broken!). A unique level set is thus not enough to locate a crack. One needs two of them. The first one denoted ϕ_n separates space into two by considering a tangent extension from the crack whereas the function ϕ_t makes it possible to locate the front. These two level sets are represented in Figure 15. The set of points characterized by $\phi_n = 0$ and $\phi_t \leq 0$ defines the position of the crack whereas points for which $\phi_n = \phi_t = 0$ defines the front. The representation of a crack by two level set functions was for the first time introduced by Stolarska et al. (2001) in 2D and Moës et al. (2002) in 3D. Figure 15 gives the iso-zero contour of both level sets for a crack in 2D. Coordinates r and θ appearing in the enrichment functions (37) are computed from the equations given in (Stolarska et al., 2001)

$$r = (\phi_n^2 + \phi_t^2)^{1/2} \quad \theta = \arctan\left(\frac{\phi_n}{\phi_t}\right) \quad (38)$$

The implicit representation is particularly interesting when the curve (surface) evolves. Indeed, contrary to the explicit representation which does not make it possible to manage topological changes easily. These changes are taken into account very naturally in the implicit level set representa-

tion. By topological changes, one understands for example the fact that two bubbles meet to form a unique bubble or the fact that a drop can separate in two drops. Another example of topological change is the case of a crack initially inside a cube (Figure 16 left) which after some propagation cuts the four faces of the cube. The crack front initially circular is split into four independent curves (Figure 16 right).

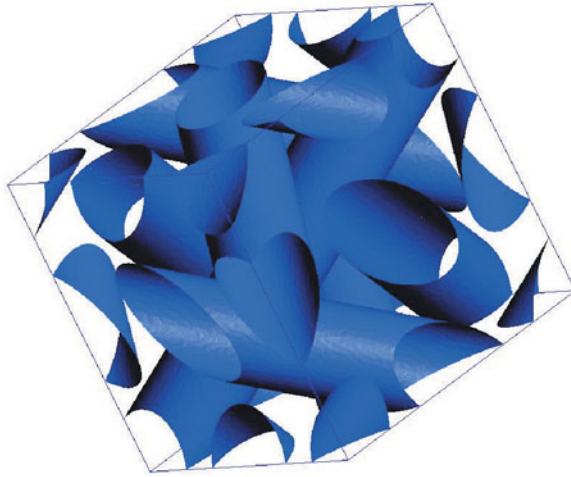


Figure 14. The iso-zero of a level set function locating the interface between strands and a matrix in a 4D composite.

The article (Osher and Sethian, 1988) was one of the first to present robust algorithms for level sets propagation. The use of the level sets for computational science then very quickly developed as attested by a sequence of three books (Sethian, 1996, 1999; Osher and Fedkiw, 2002). These algorithms of propagation were initially mainly developed within the framework of finite differences. Indeed, level sets were initially used for fluid mechanics applications: for instance to follow free interfaces or interfaces between various phases. Some articles however did develop algorithms appropriate for unstructured finite element meshes as (Barth and Sethian, 1998).

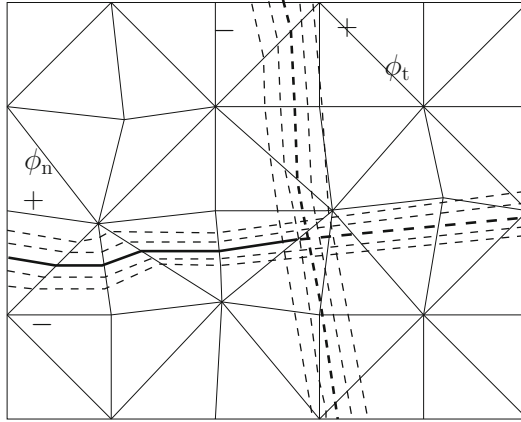


Figure 15. Two level set functions locating a crack on a 2D mesh.

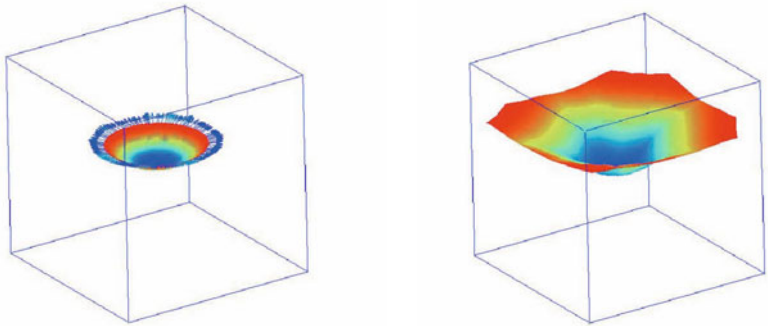


Figure 16. A lens shaped crack (left) propagating in a cube and finally cutting four cube faces (right).

4 Technical and mathematical aspects

4.1 Integration of the element stiffness

Integration on the elements cut by the crack is made separately on each side of the crack. The ϕ_n level set cuts a triangular (tetrahedral) element along a line (a plane). The possible cuts are indicated on Figures 17 and 18. For elements close to the crack tip, use of non polynomial enrichment functions requires special care (Béchet et al., 2005).

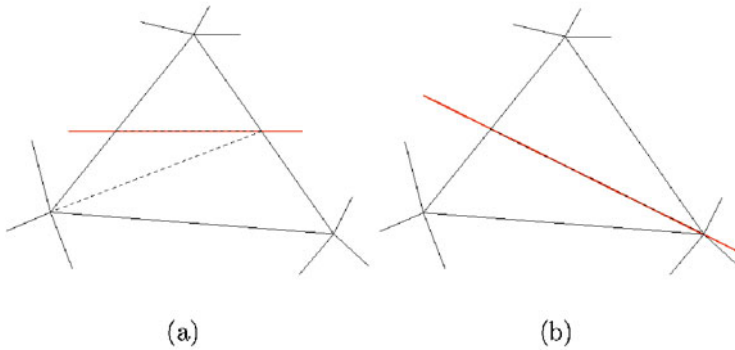


Figure 17. Two scenarios of the level set cut of a triangle.

4.2 Topological and geometrical enrichment strategies

The initial enrichment strategy for the crack tip consisted in enriching a set of nodes around the tip. A node is enriched if its support touches the crack tip (Moës et al., 1999). In 3D, nodes for which the support touches the crack front are enriched (Sukumar et al., 2000).

This type of enrichment may be called topological because it does not involve the distance from the node to the tip (front). As a matter of fact, the topological enrichment is active over an area which vanishes to zero as the mesh size goes to zero. Another enrichment, developed independently in (Béchet et al., 2005) and (Laborde et al., 2005) may be called geometrical because it consists in enriching all nodes located within a given distance to the crack tip. Both enrichment strategies are compared in Figure 19.

In order to study the influence of the enrichment on the convergence rate,

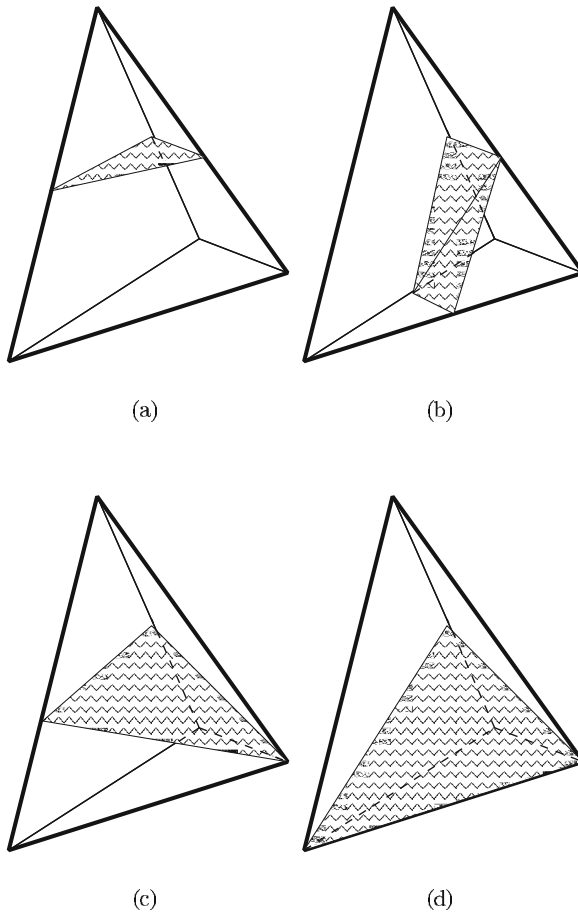


Figure 18. Four scenarios of the level set cut of a tetrahedron.

a plane strain benchmark problem is set up. A square domain in plane strain is subjected to a pure mode I. The square boundary is subjected to the exact tractions corresponding to the mode I of infinite problem. Rigid modes are prevented. The exaggerated deformed shape of the benchmark problem is shown in Figure 20. To be precise the domain size is $\Omega = [0, 1] \times [0, 1]$ and tractions applied correspond to $K_I = 1$ and $K_{II} = 0$. The crack tip is located at the center of the square. Young modulus is 1 and Poisson ratio 0. A convergence analysis is performed for a uniform grid which is recursively refined. The energy norm error, ϵ , measuring the distance between the exact, $\boldsymbol{\sigma}$, \mathbf{u} , and approximated field $\boldsymbol{\sigma}^h, \mathbf{u}^h$

$$\epsilon = \left(\frac{\int_{\Omega} (\boldsymbol{\sigma}^h - \boldsymbol{\sigma}) : \mathbf{E}^{-1} : (\boldsymbol{\sigma}^h - \boldsymbol{\sigma}) \, d\Omega}{\int_{\Omega} \boldsymbol{\sigma} : \mathbf{E}^{-1} : \boldsymbol{\sigma} \, d\Omega} \right)^{1/2} \quad (39)$$

$$= \left(\frac{\int_{\Omega} \boldsymbol{\varepsilon}(\mathbf{u}^h - \mathbf{u}) : \mathbf{E} : \boldsymbol{\varepsilon}(\mathbf{u}^h - \mathbf{u}) \, d\Omega}{\int_{\Omega} \boldsymbol{\varepsilon}(\mathbf{u}) : \mathbf{E} : \boldsymbol{\varepsilon}(\mathbf{u}) \, d\Omega} \right)^{1/2} \quad (40)$$

is plotted in Figure 21. For the topological enrichment only the nodes whose support is touching the crack tip are enriched. In the case of the geometrical enrichment, nodes within a distance of $r_e = 0.05$ from the crack tip are enriched. It can be observed that the convergence rate is 0.5 when the topological or no enrichment is present. The topological enrichment yielding however a smaller error. On the contrary, the geometrical enrichment produces a order of 1 convergence. In order to analyze these convergence rates, we must recall the convergence rate result of the classical finite element method (see for instance (Bathe, 1996))

$$\epsilon = O(h^{\min(r-m, p+1-m)}) \quad (41)$$

The regularity of the solution is indicated by r ($\mathbf{u} \in H^r(\Omega)$) whereas p is the degree of the finite element interpolation and m is the error norm used. For our benchmark, $r = 3/2$, $p = 1$ and $m = 1$, so we indeed get a convergence rate of 0.5 The topological enrichment yields a lower error than a pure FEM analysis because the X-FEM approximation spans a larger space than the FEM one. However, it does not affect the convergence rate since the enrichment area goes to zero as the mesh size goes to zero. In the case of the geometrical enrichment, the enrichment is able to represent exactly (even as h to zero) the rough part of the solution. The classical part of the approximation is thus only in charge of the smooth part of the solution yielding the optimal order of 1 convergence rate. This was proved by Laborde et al. (2005). It was also shown in this paper that (for the benchmark problem) if the polynomial approximation is raised, higher (still

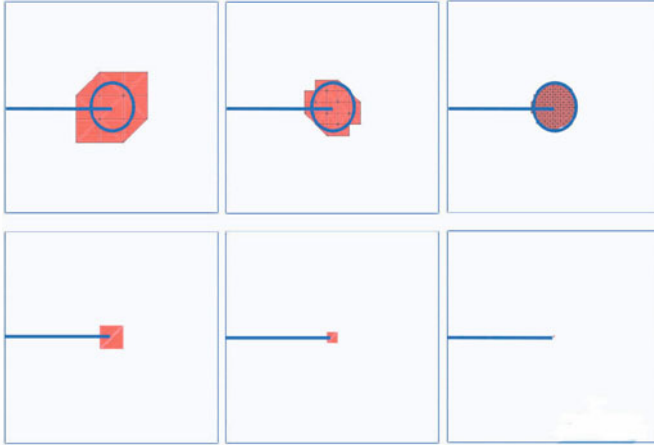


Figure 19. Extent of the enrichment zone as the mesh size decreases. Geometrical enrichment (top) and topological (bottom) enrichments are compared.

optimal) convergence rates are obtained. The polynomial degree needs only to be raised in the classical part and Heaviside parts of the approximation (first and second term term in the right hand side of (37)).

4.3 Solver and condition number

When solving a linear system of equation $Kx = f$, an important number to take into account is the condition number defined as the ratio between the maximum and minimum eigenvalue of the K matrix.

$$\kappa = \frac{\lambda_{\max}}{\lambda_{\min}} \quad (42)$$

This condition number has a direct impact on the convergence rate for an iterative solver and on the propagation of round offs for a direct solver. For instance, for the conjugate gradient iterative solver, the error at iteration m reads (Saad, 2000):

$$\|x - x_m\|_K \leq 2 \left[\frac{\sqrt{\kappa} - 1}{\sqrt{\kappa} + 1} \right]^m \|x - x_0\|_K \quad (43)$$

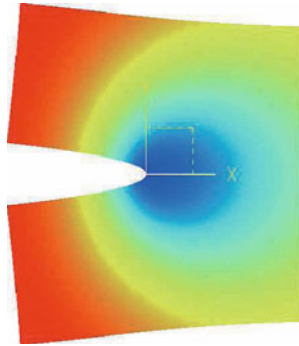


Figure 20. Mode I benchmark problem : Exaggerated deformed shape of a square slab under mode one loading.

where x_0 is the initial guess, x_m the iterate m and

$$\|a\|_K = \sqrt{a^T K a} \quad (44)$$

Thus the higher the condition number, the slower is the convergence. To be precise, the bound (43) is in general pessimistic. Indeed, first of all κ can be calculated on the basis of the eigenvalues for which the corresponding eigenvector projected on the right hand side is not zero. Then, the κ can be reajusted progressively with the iterations while being based only on the eigenvectors remaining active through the iterations (see detail in (Saad, 2000)).

The conditioning of X-FEM was studied in (Béchet et al., 2005) and (Laborde et al., 2005) for the two types of enrichment: topological and geometrical. The evolution of the condition number according to the size of elements of the grid is given in Figure 22 for the stiffness and mass matrices. They are plotted for the benchmark problem already discussed in section 4.2.

We note that for the geometrical enrichment, the condition number grows dramatically with the mesh size. A specific preconditioner was designed in (Béchet et al., 2005) to circumvent the increase. The effect of the preconditioner is also given in Figure 22. This preconditioner could be called

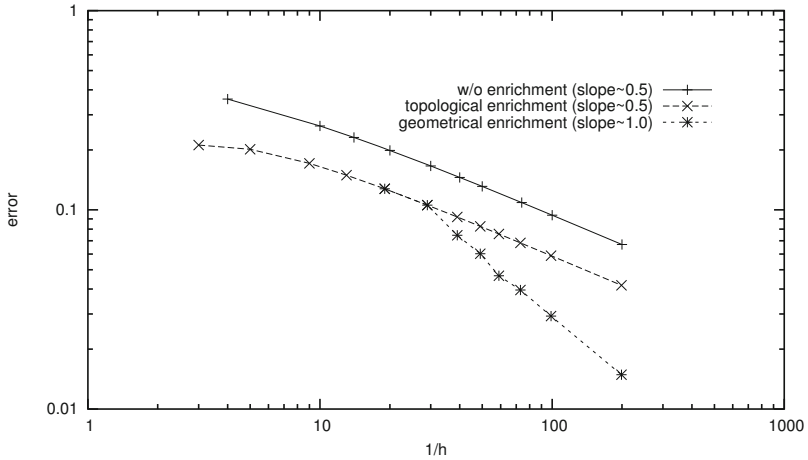


Figure 21. Relative error in the energy norm for the mode I benchmark problem. The top curve corresponds to no enrichment (slope 0.5). The middle curve is the result for the topological enrichment whereas the bottom curve (slope 1) is for the geometrical enrichment.

pre-preconditioner X-FEM preconditioner because it takes care of the specificity of X-FEM. After its application, regular FEM preconditioner may be used. The idea behind the X-FEM preconditioner is quite simple. On enriched nodes, the enriched shape functions are orthogonalized with respect to the classical shape function. The matrices related to a given node are thus diagonal.

4.4 Inf-sup condition for cracks under contact

We now consider a more complex scenario for which the crack faces may contact each other or may be loaded through hydraulic pressure for instance.

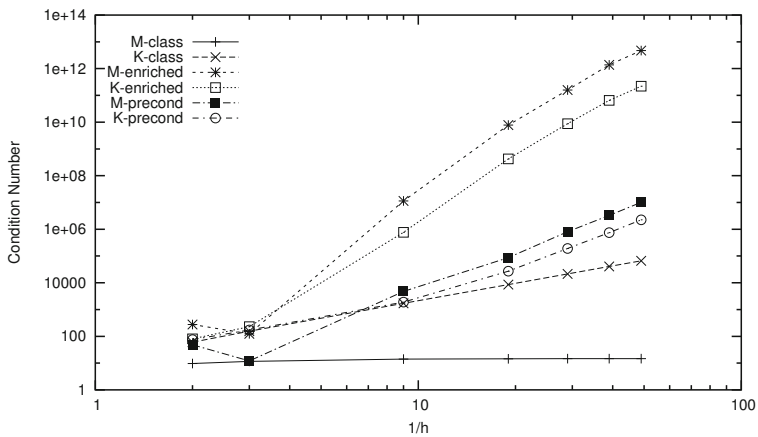
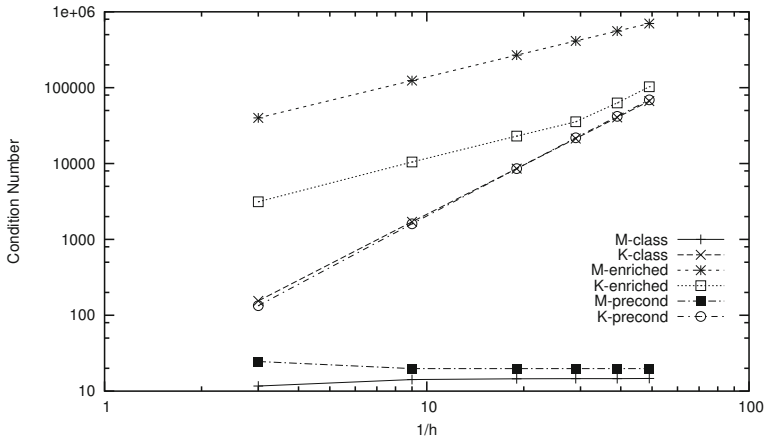


Figure 22. Condition number as a function of the mesh size for the mass and stiffness matrices. Topological (top) and geometrical (bottom) enrichments are considered as well as the influence of the preconditioner.

To take into account this more general case, we need to reconsider the mathematical formulation of the problem. The new formulation will differ from the earlier formulation (9) for which the crack faces were assumed traction free. Let \mathbf{t}^+ be the stress vector felt by the crack face S_{c^+} as shown in Figure 23.

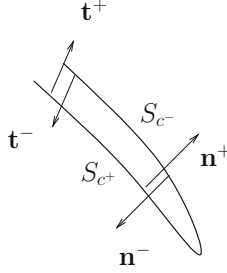


Figure 23. Notations to describe the stress vector on the cracks faces.

Due to the continuity of the stress vector across the crack, the crack S_{c^-} will feel the opposite action: $\mathbf{t}^- = -\mathbf{t}^+$. The traction free conditions (3) on the crack faces is now replaced by

$$\boldsymbol{\sigma}^+ \cdot \mathbf{n}^+ = \mathbf{t}^+ \text{ on } S_{c^+}, \quad \boldsymbol{\sigma}^- \cdot \mathbf{n}^- = -\mathbf{t}^+ \text{ on } S_{c^-} \quad (45)$$

and the corresponding variational principle now reads

$$\int_{\Omega} \boldsymbol{\varepsilon}(\mathbf{u}) : \mathbb{E} : \boldsymbol{\varepsilon}(\delta \mathbf{u}) \, d\Omega - \int_{S_{c^+}} \mathbf{t}^+ \cdot \llbracket \delta \mathbf{u} \rrbracket \, dS = \int_{S_t} \mathbf{t}^* \cdot \delta \mathbf{u} \, dS \quad \forall \delta \mathbf{u} \in U_0 \quad (46)$$

where $\llbracket \delta \mathbf{u} \rrbracket$ indicates the difference between the value of $\delta \mathbf{u}$ on S_{c^+} and S_{c^-} . To complete the formulation, we need to provide the relationship between the stress vector and the crack opening. In the case of an elastic joint gluing together both side of the crack, the relationship will simply read :

$$-\mathbf{t}^+ = k[\mathbf{u}] \quad (47)$$

where k is the “joint” stiffness. Note that the law above does not prevent the crack faces to penetrate each other, contact needs to be added.

In order to describe more complex laws on the crack faces, we shall introduce a couple of notations. The stress vector will be decomposed into its normal (scalar t_n) and tangential components (vector \mathbf{t}_τ)

$$\mathbf{t}^+ = t_n \mathbf{n}^+ + \mathbf{t}_\tau, \quad t_n = \mathbf{t}^+ \cdot \mathbf{n}^+, \quad \mathbf{t}_\tau = \mathbf{t}^+ - t_n \mathbf{n}^+ \quad (48)$$

Similarly the displacement jump is decomposed into a scalar normal jump (u_n) and tangential vectorial jump \mathbf{u}_τ

$$-\llbracket \mathbf{u} \rrbracket = u_n \mathbf{n}^+ + \mathbf{u}_\tau \quad u_n = -\llbracket \mathbf{u} \rrbracket \cdot \mathbf{n}^+, \quad \mathbf{u}_\tau = -\llbracket \mathbf{u} \rrbracket - u_n \mathbf{n}^+ \quad (49)$$

Regarding the normal part of the traction law on the interface, the most common choices are depicted in Figure 24. The cohesive type law is rather

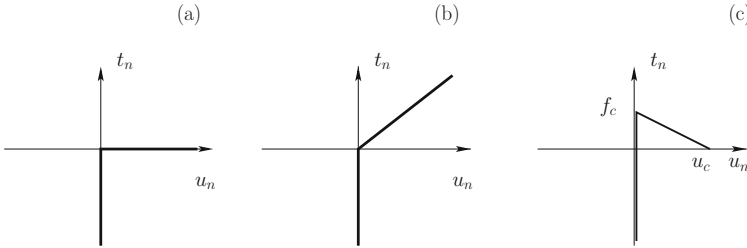


Figure 24. A set of classical normal law on the crack faces: basic contact (a), elastic interface (b), cohesive interface (c)

complex since it is non convex (t_n may not be expressed as the derivative of a convex potential in u_n). It is also irreversible in the sense that the unloading does not follow the loading curve as shown in Figure 25.

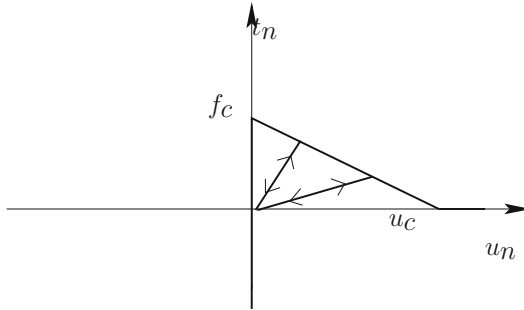


Figure 25. Cohesive law with the loading unloading depicting the gradual loss of stiffness of the interface

Regarding the tangential behavior of the interface, the case without friction leads to the nullity of the part of stress vector: $\mathbf{t}_\tau = 0$ whereas a

Coulomb friction law is driven by the following relationship

$$\mathbf{u}_\tau = \lambda \mathbf{t}_\tau, \quad \lambda \geq 0, \quad f = \|\mathbf{t}_\tau\| - \mu t_n \leq 0, \quad f\lambda = 0 \quad (50)$$

An elegant way to formulate the Coulomb friction law is through the bipotential framework introduced by (de Saxcé, 1992). Note also that the cohesive law may be extremely rich in terms of mechanical phenomena: plasticity or speed effect may be added.

Using the decomposition (48) and (49), the variational principle (46) may be rewritten as

$$\begin{aligned} \int_{\Omega} \boldsymbol{\varepsilon}(\mathbf{u}) : \mathbf{E} : \boldsymbol{\varepsilon}(\delta \mathbf{u}) \, d\Omega + \int_{S_{c+}} t_n \delta u_n \, dS + \int_{S_{c+}} \mathbf{t}_\tau \cdot \delta \mathbf{u}_\tau \, dS \\ = \int_{S_t} \mathbf{t}^* \cdot \delta \mathbf{u} \, dS \quad \forall \delta \mathbf{u} \in U_0 \end{aligned} \quad (51)$$

The variational principle (51) gives the equilibrium condition to be met for given tractions on the crack faces. Since these are unknown they will be discretized. We first consider an interface law without friction and basic contact (case a in Figure 24). Mathematically, this law is expressed locally by

$$u_n \geq 0, \quad t_n \leq 0, \quad t_n u_n = 0 \quad (52)$$

Let L be the space of regular function t_n defined on S_{c+} . The goal is to find the pair $(\mathbf{u}, t_n) \in U_0 \times L$ such that

$$\begin{aligned} \int_{\Omega} \boldsymbol{\varepsilon}(\mathbf{u}) : \mathbf{E} : \boldsymbol{\varepsilon}(\delta \mathbf{u}) \, d\Omega + \int_{S_{c+}} t_n \delta u_n \, dS &= \int_{S_t} \mathbf{t}^* \cdot \delta \mathbf{u} \, dS \quad \forall \delta \mathbf{u} \in U_0 \\ \int_{S_{c+}} \delta t_n u_n \, dS &= 0 \quad \forall \delta t_n \in L \end{aligned}$$

The above does not in fact enforce correctly contact, it enforces in fact u_n to be zero on the crack (the crack cannot open). For the above to model contact, we need to impose a priori $u_n \geq 0$ and $t_n \leq 0$ in the approximation space which is of course very cumbersome. Fortunately, we do not need these a priori assumptions by using the work of Ben Dhia et al. (2000). The contact conditions (52) may be summarized by a single (highly nonlinear) equality

$$t_n = \chi(t_n, u_n)(t_n + \beta u_n) \quad (53)$$

where β is a strictly positive parameter and

$$\chi = \chi(t_n, u_n) = 0 \quad \text{if } t_n + \beta u_n \geq 0 \quad (54)$$

$$\chi = \chi(t_n, u_n) = 1 \quad \text{if } t_n + \beta u_n < 0 \quad (55)$$

The variational principle now reads: find the pair $(\mathbf{u}, t_n) \in U_0 \times L$ such that

$$\begin{aligned} \int_{\Omega} \boldsymbol{\varepsilon}(\mathbf{u}) : \mathbf{E} : \boldsymbol{\varepsilon}(\delta \mathbf{u}) + \beta \chi u_n \delta u_n \, d\Omega \\ + \int_{S_{c+}} \chi t_n \delta u_n \, dS = \int_{S_t} \mathbf{t}^* \cdot \delta \mathbf{u} \, dS \quad \forall \delta \mathbf{u} \in U_0 \\ \int_{S_{c+}} \chi \delta t_n u_n + \frac{(\chi - 1)}{\beta} t_n \delta t_n \, dS = 0 \quad \forall \delta t_n \in L \end{aligned}$$

In the system above, spaces U and L no longer involve sign conditions and we may proceed to the space discretization. The X-FEM discrete displacement space U_0^h has already been described earlier. Regarding the discrete pressure space L , extra care needs to be taken in order to satisfy the so-called Inf-Sup Babuska-Brezzi condition.

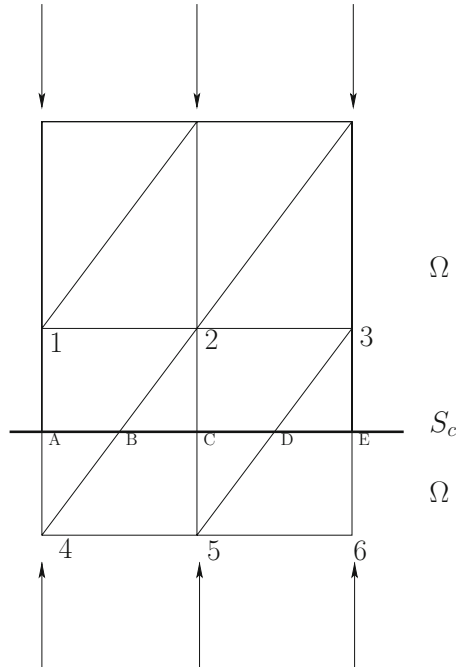


Figure 26. A crack cutting a mesh.

To illustrate the problem, consider the rectangular domain depicted in

Figure 26 (fully) cut by a crack. The two parts of the domain are pressed towards each other. It is tempting to discretize t_n based on the 1D mesh on S_c with 5 “nodes”, labelled A to E . Unfortunately, this yield highly oscillatory pressure t_n over S_c (Ji and Dolbow, 2004; Moës et al., 2006). If the mesh is refined, the oscillatory behavior may even get worse. This oscillatory behavior is to be related to locking issue similar to what happens in incompressible formulation when the pressure is too rich and creates checkerboard type patterns. This problem is specific to the X-FEM because the crack lays inside the element. If the crack is meshed, this issue does not appear. A set of papers have been devoted to alleviate this locking issue, following different strategies

- following a Nitsche type approach (Nitsche, 1971; Hansbo and Hansbo, 2002, 2004)
- following a residual-free bubble stabilization approach (Mourad et al., 2007; Dolbow and Franca, 2008)
- following a Barbosa and Hugues type stabilization of the Lagrange multipliers (Haslinger and Renard, 2008)
- using a mortar based approach (Kim et al., 2007)
- proper choice of the Lagrange multiplier space (Moës et al., 2006), (Géniaut et al., 2007) and more recently (Béchet et al., 2009).

We will now detail the later paper (Béchet et al., 2009) which is particularly attractive because the pressure field is discretized using the same nodes as the displacement field. The nodes of all element cut by the crack will bear a pressure t_n degree of freedom (these nodes are numbered from 1 to 6 in Figure 26). It was proved in (Béchet et al., 2009) that by applying specific ties between the pressure degrees of freedom, the inf-sup was fulfilled.

The algorithm to create the ties goes as follows. Let E be the set of edges cut by the crack. We pick in E a set of independent edges. Two edges are said to be independent if they do not share a common nodes. Note that the choice of independent edges is not unique. In Figure 26, the set may be for instance (2,4),(3,5) or (1,4),(3,5) or even (1,4),(2,5),(3,6). On the more complex mesh depicted in Figure 27, a possible set of independent edges is indicated by dots (and square at the end nodes).

The pressure degrees of freedom at the end nodes of each independent edge are forced to be equal. These is illustrated by the numbers which are the same on Figure 27 (top), for the end nodes of each independent edge.

Once the independent edges have been selected, some nodes of edges in E may not have been taken care of. This is the case for the circled nodes in Figure 27 (bottom). The pressure field at these nodes is linked to the value at the squared nodes to which it is connected to through an edge in E

(when the squared are multiple, either one is picked or a linear combination may be built with coefficients forming a partition of unity (Béchet et al., 2009)). The algorithm described above may also be applied in 3D.

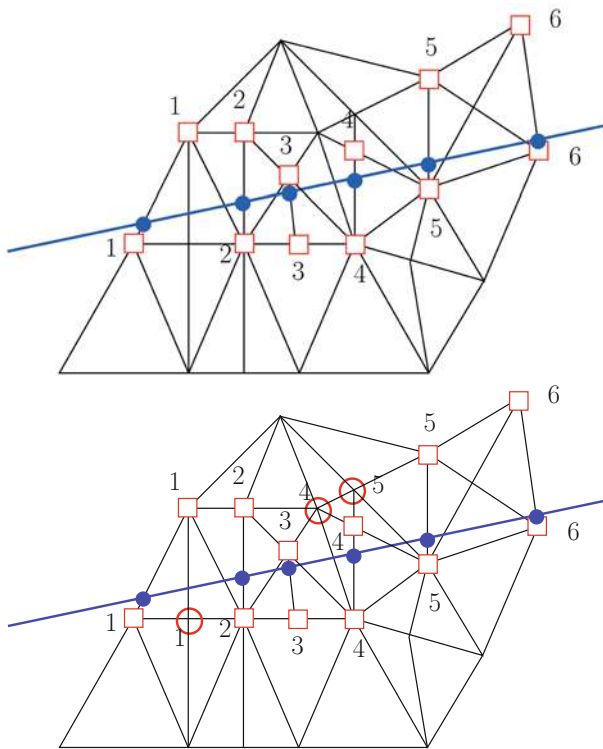


Figure 27. (Top) Selection of the independent edges. These edges are in between square nodes. The connected squared nodes will have the same pressure degree of freedom. (Bottom) Isolated nodes are located by circle nodes. Their pressure degree of freedom is forced equal to the one of a square they can connect to through a cut edge.

5 Configurational analysis of the crack front

5.1 The Eshelby tensor

Eshelby tensor is a second order tensor generally non symmetric defined by

$$P_{ij} = w\delta_{ij} - \sigma_{kj}u_{k,i}, \quad w = \frac{1}{2}\sigma_{kl}\epsilon_{kl} \quad (56)$$

in the case of small strain linear elasticity.

This tensor is a so called configurational tensor because it gives information on the change of energy in a system when its configuration is changed. Consider the clamped domain shown at the top in Figure 28. If a part of the domain is taken out (middle Figure), the energy in the system will change.

Let us assume that we keep removing material with a velocity of material retrieval \mathbf{v} (bottom Figure 28). The rate of loss of potential energy is given by (in tensorial and indicial notations) by

$$\dot{U} = \int_S \mathbf{v} \cdot \mathbf{P} \cdot \mathbf{n} \, dS = \int_S v_i P_{ij} n_j \, dS \quad (57)$$

where \mathbf{n} is the outer normal.

Since the boundary of the material being retrieved is traction free ($\sigma_{ij}n_j = 0$) the integrand above reduces simply to $-w \|\mathbf{v}\|$ which is indeed negative implying a drop of potential energy in the system. The drop value is simply related to the elastic energy density present before the advance of the front. Again, we stress the fact that this simple expression was obtained on a traction free boundary. More complex expressions arise in the case of loaded boundaries and the general formula (57) must then be used.

Imagine now that the growing front depicted in Figure 28 (bottom) does not remove material but replaces a material with another one (phase change). We obtain then picture 29. The change in potential energy now reads

$$\dot{U} = \int_S \mathbf{v} \cdot \llbracket \mathbf{P} \rrbracket \cdot \mathbf{n} \, dS \quad (58)$$

The jump denoting the Eshelby tensor on right before the front minus the one right behind the front. This jump will be zero if the two material phases are identical. Indeed, replacing a material by the same one does not change at all the configuration and thus the potential energy.

The Eshelby tensor gives information on the change of energy in a system due to a change of configuration. On the other hand the Cauchy stress tensor gives information in the change of energy in system due to a change in spatial location. To understand this, consider now in Figure 28 (bottom) that the velocity \mathbf{v} is an imposed velocity on the particles of the domain

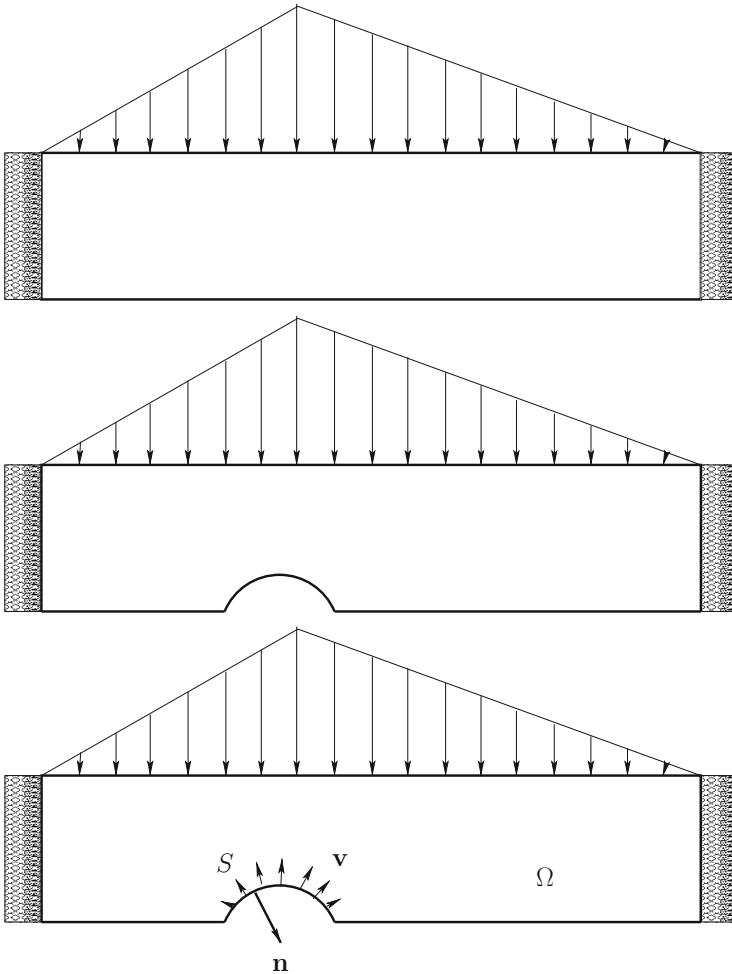


Figure 28. Top: a clamped domain subjected to some loadings, middle: the same loading applied to a different configuration, bottom: this Figure represents a spatial or configurational velocity on the boundary of the domain.

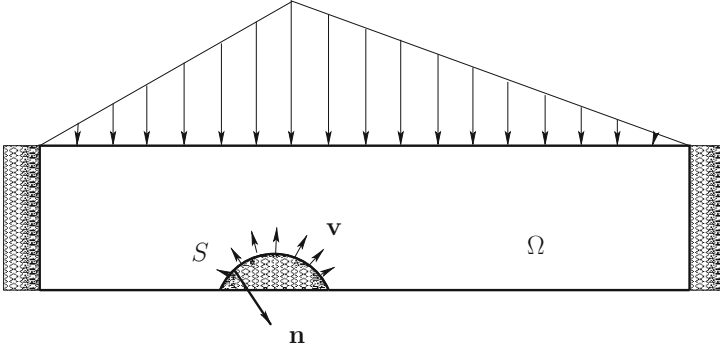


Figure 29. The clamped domain with a material interface.

(and no longer a rate at which material is being removed). This imposed velocity will generate stresses. The change in potential now reads

$$\dot{U} = \int_S \mathbf{v} \cdot \boldsymbol{\sigma} \cdot \mathbf{n} \, dS = \int_S v_i \sigma_{ij} n_j \, dS \quad (59)$$

The similarity with (57) is clear.

If we now consider Figure 29 a material interface being pushed (we are not talking about a phase change but the fact that the interface is being pushed at some velocity). The change in energy reads

$$\dot{U} = \int_S \mathbf{v} \cdot \llbracket \boldsymbol{\sigma} \rrbracket \cdot \mathbf{n} \, dS \quad (60)$$

The jump term $\llbracket \boldsymbol{\sigma} \rrbracket \cdot \mathbf{n}$ is the reaction to the imposed velocity.

Assuming the stress $\boldsymbol{\sigma}$, strain $\boldsymbol{\varepsilon}$ and displacement \mathbf{u} fields satisfy elasticity equations (equilibrium, compatibility and constitutive behavior) :

$$\sigma_{ij,j} = 0 \quad \epsilon_{ij} = \frac{1}{2}(u_{i,j} + u_{j,i}) \quad \sigma_{ij} = E_{ijkl} \epsilon_{kl} \quad (61)$$

the Eshelby tensor is divergence free

$$\nabla \cdot \mathbf{P} = 0, \quad P_{ij,j} = 0 \quad (62)$$

5.2 Energy integrals

The fact that the Eshelby tensor is divergence free means that over any closed contour S the following integral is zero

$$\int_S \mathbf{P} \cdot \mathbf{n} \, dS \quad (63)$$

where \mathbf{n} is the outward normal to the contour. In fact, the assertion is true provided the domain described by the close contour has a smooth and continuous solution (and thus the divergence theorem may be applied). In other words the expression above is wrong if the contour S surrounds a crack tip. The integral (a related version to be precise) will be however very useful to characterize the strength of the singularity.

Next, we show that even though the integral around a crack tip is not zero, the result obtained will be the same whatever the contour chosen. More precisely, we have the following property introduced by Rice.

$$J = \int_{S_1} \mathbf{q} \cdot \mathbf{P} \cdot \mathbf{n}_1 \, dS_1 = \int_{S_2} \mathbf{q} \cdot \mathbf{P} \cdot \mathbf{n}_2 \, dS_2 \quad (64)$$

The contour S_1 and S_2 are depicted by dashed lines in Figure 30. The vector \mathbf{q} is a vector indicating the direction of the crack (assumed straight at this point). To prove (64), we first define Ω_{12} as the domain bounded by S_1 , S_2 , S_{12c+} and S_{12c-} . Over the Ω_{12} , the mechanical field are smooth and we may apply the divergence theorem:

$$\int_{S_1 \cup S_2 \cup S_{12c+} \cup S_{12c-}} \mathbf{q} \cdot \mathbf{P} \cdot \mathbf{n} \, dS = \mathbf{q} \cdot \int_{\Omega_{12}} \nabla \cdot \mathbf{P} \, d\Omega = 0 \quad (65)$$

where \mathbf{n} is the outward normal to Ω_{12} . Since \mathbf{n} and \mathbf{q} are orthogonal over $S_{12c+} \cup S_{12c-}$ and the traction is free over these segments, we have

$$\mathbf{q} \cdot \mathbf{P} \cdot \mathbf{n} = 0 \text{ on } S_{12c+} \cup S_{12c-} \quad (66)$$

yielding (64).

The physical meaning of the J integral is the power dissipated as the crack tip advances with the speed \mathbf{q} . Rice did show that J was related in linear elasticity to the stress intensity factor of the crack (for a unit crack tip velocity).

$$J = \frac{(1 - \nu^2)}{E} (K_I^2 + K_{II}^2) + \frac{1}{2\mu} K_{III}^2 \quad (67)$$

The contour integral (64) may be transformed into a so-called domain integral Destuynder et al. (1983). In order to perform the transition from

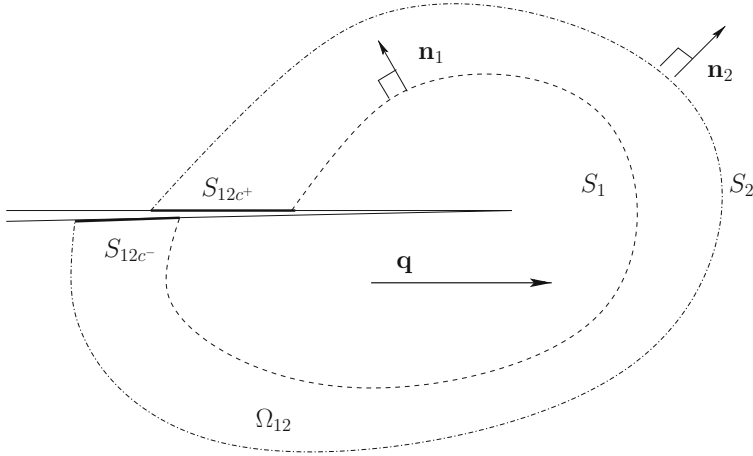


Figure 30. Notations to prove the J-rice contour independence property.

a contour to a domain integral, let us change slightly the definition of the virtual velocity \mathbf{q} . It is a unit vector aligned with the crack within the contour S_0 and it drops to zero on the contour S , see Figure 31. We may write

$$J = \int_{S_0} \mathbf{q} \cdot \mathbf{P} \cdot \mathbf{n}_0 \, dS + \int_S \mathbf{q} \cdot \mathbf{P} \cdot \mathbf{n} \, dS = - \int_{\Omega} \nabla \cdot (\mathbf{q} \cdot \mathbf{P}) \, d\Omega = - \int_{\Omega} \nabla \mathbf{q} : \mathbf{P} \, d\Omega \quad (68)$$

Thus

$$J = - \int_{\Omega} \nabla \mathbf{q} : \mathbf{P} \, d\Omega \quad (69)$$

The domain Ω in the above is the domain enclosed by the contour S , since in the proof (68), the contour S_0 may be taken as small as one wishes around the tip. Compared to (64), the domain integral (69) is much more appropriate to finite element computations since the domain integral may be split as integral over elements. In fact, only one layer of elements do contribute to the integral as depicted in Figure 32 since the over the inner elements of the domain the \mathbf{q} field is uniform.

5.3 Energetic information for cohesive cracks

So far, we discussed only straight traction free crack. Let us now consider that the crack faces are no longer traction free due to a contact or the

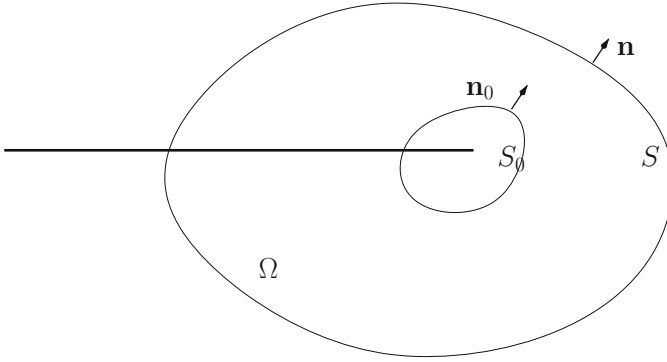


Figure 31. Notations for the domain integral proof.

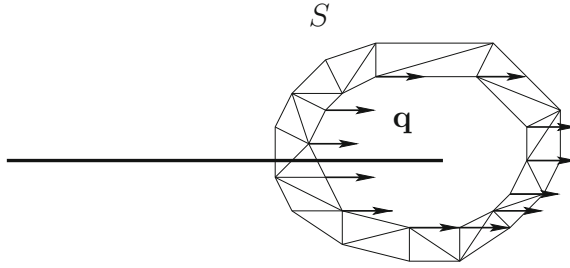


Figure 32. Elements contributing to the J domain integral.

presence of a cohesive zone. The J domain integral (69) (or its contour expression (64)) is then no longer contour independent. Independence may be regained by adding a boundary term to the J integral on the crack faces enclosed by the domain (contour). The more general expression is

$$J = \underbrace{- \int_{\Omega} \nabla \mathbf{q} : \mathbf{P} \, d\Omega}_{J_{\Omega}} + \underbrace{\int_{S_{c+} \cup S_{c-}} \mathbf{q} \cdot \mathbf{P} \cdot \mathbf{n} \, dS}_{J_{\text{coh}}} \quad (70)$$

In order to show the domain independency, we use the notation depicted

in Figure 33. We need to show that

$$\begin{aligned}
 - \int_{\Omega_1} \nabla \mathbf{q} : \mathbf{P} \, d\Omega + \int_{S_{1c+} \cup S_{1c-}} \mathbf{q} \cdot \mathbf{P} \cdot \mathbf{n} \, dS = \\
 - \int_{\Omega_2} \nabla \mathbf{q} : \mathbf{P} \, d\Omega + \int_{S_{2c+} \cup S_{2c-}} \mathbf{q} \cdot \mathbf{P} \cdot \mathbf{n} \, dS \quad (71)
 \end{aligned}$$

The notations are detailed in Figure 33. Removing the contribution from the domain Ω_0 from both sides, we get.

$$\begin{aligned}
 - \int_{\Omega_1 \setminus \Omega_0} \nabla \mathbf{q} : \mathbf{P} \, d\Omega + \int_{S_{1c+} \cup S_{1c-} \setminus S_{0c+} \cup S_{0c-}} \mathbf{q} \cdot \mathbf{P} \cdot \mathbf{n} \, dS = \\
 - \int_{\Omega_2 \setminus \Omega_0} \nabla \mathbf{q} : \mathbf{P} \, d\Omega + \int_{S_{2c+} \cup S_{2c-} \setminus S_{0c+} \cup S_{0c-}} \mathbf{q} \cdot \mathbf{P} \cdot \mathbf{n} \, dS \quad (72)
 \end{aligned}$$

Applying the divergence theorem on both sides and owing to the fact that the Eshelby tensor is divergence free, we get the proof.

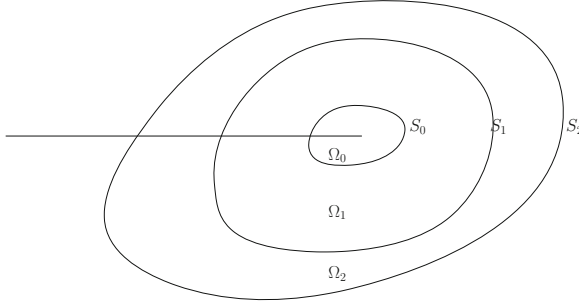


Figure 33. Notations to prove the J domain integral independency in the case of cohesive cracks. The domains Ω_i , $i = 1, \dots, 3$ are enclosed by the contours S_i , $i = 1, \dots, 3$. Similarly, the notation S_{ic+} denotes the part of the crack enclosed by the contour S_i .

In the case of a cohesive crack it is interesting to detail the expression

of the boundary term.

$$J_{\text{coh}} = \int_{S_{c^+} \cup S_{c^-}} \mathbf{q} \cdot \mathbf{P} \cdot \mathbf{n} \, dS \quad (73)$$

$$= \int_{S_{c^+}} (\mathbf{q} \cdot \nabla \mathbf{u}^+) \cdot (\boldsymbol{\sigma}^+ \cdot \mathbf{n}^+) \, dS + \quad (74)$$

$$\int_{S_{c^-}} (\mathbf{q} \cdot \nabla \mathbf{u}^-) \cdot (\boldsymbol{\sigma}^- \cdot \mathbf{n}^-) \, dS \quad (75)$$

$$= - \int_0^l \mathbf{t}^+ \frac{d[\mathbf{u}]}{ds} \, ds \, \|\mathbf{q}\| \quad (76)$$

$$= - \int_0^{u_c} t_n \, du_n \, \|\mathbf{q}\| \quad (77)$$

The last inequality was obtained assuming no friction on the crack faces. The boundary term is thus negative and is the opposite of the area under the cohesive law (value $-0.5f_c u_c$ is we consider the cohesive law depicted in Figure 25. The value of the J domain integral is zero for a cohesive crack since there is no singularity at the crack tip, we thus have

$$J = 0 = \underbrace{J_\Omega}_{\geq 0} + \underbrace{J_{\text{coh}}}_{\leq 0} \quad (78)$$

The J_Ω part is positive and represents the strength of the singularity at the crack tip if all cohesive forces were removed. The cohesive forces do create an opposite singularity. Even though no singularity exist at the tip of a cohesive crack, the stress field at some distance of the crack tip (larger than the cohesive zone length) behave as if there was a singularity (K dominance zone). The integral J_Ω is able to compute the strength of this K field. Note that the integral J_Ω is domain independant provided the domain always embeds fully the cohesive zone.

Finally, the condition $J = 0$ may be used as a robust way to find the proper load for a given extent of the cohesive zone as in (Moës and Belytschko, 2002). Since cohesive crack do not yield a singular field, the tip enrichment described in (37) is not appropriate. Non singular tip functions may be used as described in (Zi and Belytschko, 2003) or (Moës and Belytschko, 2002). Some authors prefer to consider only the Heaviside enrichment so that elements are either not cut or completely cut: (Wells and Sluys, 2001), (Mergheim et al., 2005) and (Meschke and Dumstorff, 2007).

Bibliography

- I. Babuška and I. Melenk. Partition of unity method. *International Journal for Numerical Methods in Engineering*, 40(4):727–758, 1997.
- I. Babuška and M. Rosenzweig. A finite element scheme for domains with corners. *Numer. Math.*, 20:1–21, 1972.
- T. J. Barth and J. A. Sethian. Numerical schemes for the Hamilton-Jacobi and level set equations on triangulated domains. *Journal of Computational Physics*, 145(1):1–40, 1998.
- K. J. Bathe. *Finite element procedures*. Prentice-Hall, 1996.
- E. Béchet, H. Minnebo, N. Moës, and B. Burgardt. Improved implementation and robustness study of the x-fem method for stress analysis around cracks. *International Journal for Numerical Methods in Engineering*, 64: 1033–1056, 2005.
- E. Béchet, N. Moës, and B. Wohlmuth. A stable lagrange multiplier space for stiff interface condition within the extended finite element method. *International Journal for Numerical Methods in Engineering*, 78:931–954, 2009.
- T. Belytschko and T. Black. Elastic crack growth in finite elements with minimal remeshing. *International Journal for Numerical Methods in Engineering*, 45(5):601–620, 1999.
- T. Belytschko and M. Fleming. Smoothing, enrichment and contact in the element-free galerkin method. *Computers and Structures*, 71(2):173–195, 1999.
- T. Belytschko, Y.Y. Lu, and L. Gu. Element-free galerkin methods. *International Journal for Numerical Methods in Engineering*, 37:229–256, 1994.
- H. Ben Dhia, I. Vautier, and M. Zarroug. Problèmes de contact frottant en grandes transformations: du continu au discret. *Revue Européenne des éléments finis*, 9:243–261, 2000.
- G. de Saxcé. A generalization of Fenchel’s inequality and its applications to constitutive law. *Compte-Rendus Acad. Sci. Paris, Série II*, 314:125–129, 1992.
- P. Destuynder, M. Djaoua, and S. Lescure. Some remarks on elastic fracture mechanics (quelques remarques sur la mécanique de la rupture élastique). *Journal de Mécanique théorique et appliquée*, 2(1):113–135, 1983.
- J.E. Dolbow and L.P. Franca. Residual-free bubbles for embedded dirichlet problems. *Comp. Meth. in Applied Mech. and Engrg.*, 197:3751–3759, 2008.
- C.A.M. Duarte and J.T. Oden. An hp meshless method. *Numerical methods for partial differential equations*, 12:673–705, 1996.

- M. Fleming, Y. A. Chu, B. Moran, and T. Belytschko. Enriched element-free Galerkin methods for crack tip fields. *International Journal for Numerical Methods in Engineering*, 40(8):1483–1504, 1997.
- S. Géniaut, P. Massin, and N. Moës. A stable 3D contact formulation for cracks using x-fem. *Revue européenne de mécanique numérique*, 16:259–276, 2007.
- P. Grisvard. *Elliptic Problems in Nonsmooth Domains*. Pitman Publishing, Inc, Boston, 1985.
- A. Hansbo and P. Hansbo. An unfitted finite element method, based on Nitsche’s method, for elliptic interface problems. *Computer Methods In Appl. Mechanics Engineering*, 191:5537–5552, 2002.
- A. Hansbo and P. Hansbo. A finite element method for the simulation of strong and weak discontinuities in solid mechanics. *Computer Methods In Applied Mechanics And Engineering*, 193:3523–3540, 2004.
- J. Haslinger and Y. Renard. A new fictitious domain approach inspired by the extended finite element method. *SIAM Journal of numerical analysis*, 47:1474–1499, 2009.
- H. Ji and J.E. Dolbow. On strategies for enforcing interfacial constraints and evaluating jump conditions with the extended finite element method. *International Journal for Numerical Methods in Engineering*, 61:2508–2535, 2004.
- T. Y. Kim, J. Dolbow, and T. Laursen. A mortared finite element method for frictional contact on arbitrary interfaces. *Computational Mechanics*, 39(3):223–235, 2007.
- P. Krysl and T. Belytschko. Element free Galerkin method for dynamic propagation of arbitrary 3-d cracks. *International Journal for Numerical Methods in Engineering*, 44(6):767–800, 1999.
- P. Laborde, J. Pommier, Y. Renard, and M. Salaun. High-order extended finite element method for cracked domains. *International Journal for Numerical Methods in Engineering*, 64:354–381, 2005.
- W.K. Liu, J. Adee, S. Jun, and T. Belytschko. Reproducing kernel particle methods for elastic and plastic problems. *Am Soc Mech Eng Appl Mech Div AMD*, 180:175–189, 1993.
- J.M. Melenk and I. Babuška. The partition of unity finite element method: Basic theory and applications. *Comp. Meth. in Applied Mech. and Eng.*, 39:289–314, 1996.
- J. Mergheim, E. Kuhl, and P. Steinmann. A finite element method for the computational modelling of cohesive cracks. *Int. J. For Numerical Methods In Engineering*, 63(2):276–289, 2005.
- G. Meschke and P. Dumstorff. Energy-based modeling of cohesive and cohesionless cracks via X-FEM. *Computer Methods In Appl. Mechanics Engineering*, 196(21-24):2338–2357, 2007.

- N. Moës and T. Belytschko. Extended finite element method for cohesive crack growth. *Engineering Fracture Mechanics*, 69:813–834, 2002. URL [http://dx.doi.org/10.1016/S0013-7944\(01\)00128-X](http://dx.doi.org/10.1016/S0013-7944(01)00128-X).
- N. Moës, J. Dolbow, and T. Belytschko. A finite element method for crack growth without remeshing. *International Journal for Numerical Methods in Engineering*, 46:131–150, 1999.
- N. Moës, A. Gravouil, and T. Belytschko. Non-planar 3D crack growth by the extended finite element and level sets. part I: Mechanical model. *International Journal for Numerical Methods in Engineering*, 53:2549–2568, 2002.
- N. Moës, M. Cloirec, P. Cartraud, and J.-F. Remacle. A computational approach to handle complex microstructure geometries. *Comp. Meth. in Applied Mech. and Engrg.*, 192:3163–3177, 2003. URL [http://dx.doi.org/doi:10.1016/S0045-7825\(03\)00346-3](http://dx.doi.org/doi:10.1016/S0045-7825(03)00346-3).
- N. Moës, E. Béchet, and M. Tourbier. Imposing essential boundary conditions in the extended finite element method. *International Journal for Numerical Methods in Engineering*, 67:1641–1669, 2006.
- N. Molino, Z. Bao, and R. Fedkiw. A virtual node algorithm for changing mesh topology during simulation. *SIGGRAPH, ACM TOG 23*, pages 385–392, 2004.
- H. M. Mourad, J. Dolbow, and I. Harari. A bubble-stabilized finite element method for Dirichlet constraints on embedded interfaces. *Int. J. For Numerical Methods In Engineering*, 69(4):772–793, 2007.
- B. Nayroles, G. Touzot, and P. Villon. Generalizing the finite element method: Diffuse approximation and diffuse elements. *Computers and Structures*, 10(5):307–318, 1992.
- J. Nitsche. Über ein Variationsprinzip zur lösung von Dirichlet-problemen bei Verwendung von Teilräumen, die keinen Randbedingungen unterworfen sind. *Abhandlungen aus dem Mathematischen Seminar des Universität Hamburg*, 36:9–15, 1971.
- S. Osher and R. Fedkiw. *Level set methods and dynamic implicit surfaces*. Springer Verlag, 2002.
- S. Osher and J. A. Sethian. Fronts propagating with curvature-dependent speed: Algorithms based on Hamilton-Jacobi formulations. *Journal of Computational Physics*, 79(1):12–49, November 1988.
- Y. Saad. *Iterative methods for sparse linear systems*. PWS Publishing company, third edition edition, 2000.
- J. A. Sethian. *Level Set Methods & Fast Marching Methods: Evolving Interfaces in Computational Geometry, Fluid Mechanics, Computer Vision, and Materials Science*. Cambridge University Press, Cambridge, UK, 1999.

- J.A. Sethian. *Level Set Methods: Evolving Interfaces in Computational Geometry, Fluid Mechanics, Computer Vision, and Materials Science*. Cambridge Monographs on Applied and Computational Mathematics, 1996.
- J.H. Song, P.M.A. Areais, and T. Belytschko. A method for dynamic crack and shear band propagation with phantom nodes. *International Journal for Numerical Methods in Engineering*, 67:868–893, 2006.
- M. Stolarska, D. L. Chopp, N. Moës, and T. Belytschko. Modelling crack growth by level sets and the extended finite element method. *International Journal for Numerical Methods in Engineering*, 51(8):943–960, 2001.
- T. Strouboulis, I. Babuška, and K. Copps. The design and analysis of the generalized finite element method. *Comp. Meth. in Applied Mech. and Engrg.*, 181:43–71, 2000.
- N. Sukumar, N. Moës, T. Belytschko, and B. Moran. Extended Finite Element Method for three-dimensional crack modelling. *International Journal for Numerical Methods in Engineering*, 48(11):1549–1570, 2000.
- G.N. Wells and L.J. Sluys. A new method for modelling cohesive cracks using finite elements. *International Journal for Numerical Methods in Engineering*, 50:2667–2682, 2001.
- G. Zi and T. Belytschko. New crack-tip elements for XFEM and applications to cohesive cracks. *International Journal for Numerical Methods in Engineering*, 57:2221–2240, 2003.